Applied Physics Express 12, 095502 (2019)
https://doi.org/10.7567/1882-0786/ab389f

LETTER

Broadside circularly-polarized radiation generated by surface wave diffraction

Bo Wang[1], Hang Wong[2*], Di Wu[3], and Kwan L. Yeung[1]

[1]Department of Electrical and Electronic Engineering, The University of Hong Kong, Hong Kong, 99077, People's Republic of China
[2]State Key Laboratory of Terahertz and Millimeter Waves, Department of Electronic Engineering, City University of Hong Kong, Hong Kong, 999077, People's Republic of China
[3]College of Electronic Science and Technology, Shenzhen University, Shenzhen, 518060, People's Republic of China

*E-mail: hang.wong@cityu.edu.hk

Received July 8, 2019; revised July 27, 2019; accepted August 5, 2019; published online August 14, 2019

Conventionally, the surface wave radiation enabled by periodic structures which generate a leaky mode with the propagation constant at its −1 harmonic requires a large-size radiator and a complicated dispersion control in geometrical shapes. In this work, we exhibit a method of implementing surface wave radiation by predetermined diffractions. It applies dielectric truncation along the circumference as diffraction discontinuities without periodic structures involved. We demonstrate that the spatial distributions of the emitted radiations and the polarization of the electric field can be controlled through the manipulation in amplitude and phase of the surface wave diffraction.

Surface wave (SW) is widely observed from ultra-low frequency supported by the earth surface[1)] to as high as optical frequency supported on highly conducting surfaces.[2)] This kind of slow wave now plays a key role in the wide frequency spectrum such as plasmonics,[3,4)] spoof surface plasmon (SSP),[5–11)] metamaterials, nano-photonics,[12)] and satellite communications.[13)] SW propagation can generate wave radiation in a desirable direction through the means of discontinuities,[14)] bends,[15)] surface texture,[10,14,16)] or periodic structures. Synthetic patterns generated from the surface wave are useful in various applications including object tracking, speed detection, anti-collision, leakage detection, chip-to-chip communication, and high-speed radio.

The approach of using periodic structures is a flexible and effective tool in manipulating the guided SW's propagation constant in its −1 harmonic[14)] whose dispersion curve has potential to locate in the leaky mode region. The periodic structures can be formed by modulated artificial impedance surfaces,[17–19)] SSP radiators[5–7,20)] and holographic surface.[13,17–19)] These modulated surfaces can concentrate the spatial energy from SW radiation at a desired direction, or shape the radiation pattern on diverse rigorous objects. Simultaneous radiation manipulation of both the beam pointing and radiated polarization requires an extra tunable dimension, which is usually implemented using anisotropic surfaces with tensor impedance properties[17)] to separately control the $\boldsymbol{E}$ field components of the SW radiation. Nevertheless, the periodic structure for the SW radiation needs to satisfy the condition of pure traveling-wave and a series of meticulously planned dispersion constants. This approach for SW radiation requires a large size, time-consuming unit cell data collection, and complicated structure with a lower robustness. The anisotropic surfaces, derived from periodic structures, even suffer a severer situation.

Unlike the conventional approach to generate SW radiation in a leaky mode, we introduce a method of controlling SW radiation by applying wave diffractions via manipulating the phase distribution on a dielectric slab. Our proposed unique structure of the dielectric slab truncation produces a synthesized radiation with only terminal diffractions avoiding complicated periodic structures. The generated SW through our proposed methodology is similar with the normal currents that typically occur on electric conductor,[21)] so a simple method with equivalent currents to evaluate the radiation property of SWs is presented in this letter. The proposed structure is simple and low-profile, which is composed of a centre-fed probe and a grounded dielectric slab (GDS) with Archimedean-spiral shape. The centre-fed probe acts as a RF power source to generate the surface wave mode (SWM) and the GDS is designed to guide only the fundamental SW mode, TM_0. However, the transverse phase velocity of the propagating surface wave is larger than that of the free space, so there is no leaky wave excited on the SWM traveling. Until the propagating energy hits the discontinuity at the dielectric truncation, diffraction radiation of SW appears. Furthermore, the small surface wave diffraction radiation (SWDR) areas near truncation can be regarded as radially directed currents with their phase manipulated by the radii of the dielectric slab. The amplitude and phase varied with radii are analyzed through a simple circular plate to guide the design of Archimedean spiral. Finally, we demonstrate the synthesis of surface wave diffractions, both analytically and experimentally, on the object of broadside radiation with circular polarization (CP).

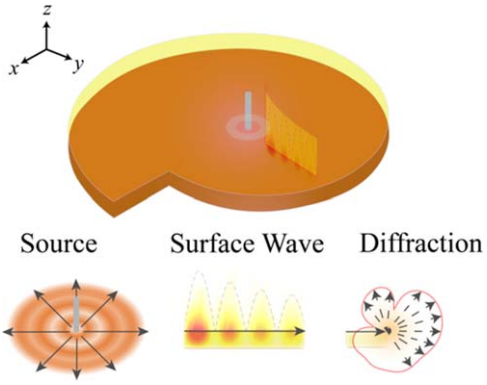

Fig. 1. (Color online) A general view of the proposed surface wave diffraction radiator.

Figure 1 shows the Archimedean spiral shaped GDS with phase-reversal geometric truncation to generate the broadside radiation. The diffractions on the dielectric edge can be viewed as radiators to transfer SWMs into radiation modes. The value of the radii can be employed to control the phase of the radiator.

To illustrate the design above, we begin with a simple model shown in Fig. 2(a). The axially symmetric GDS is set

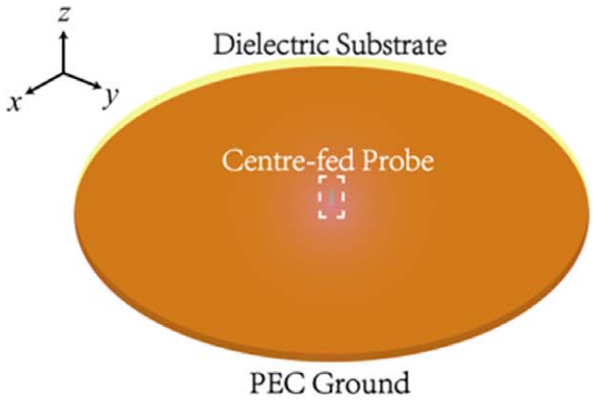

(a)

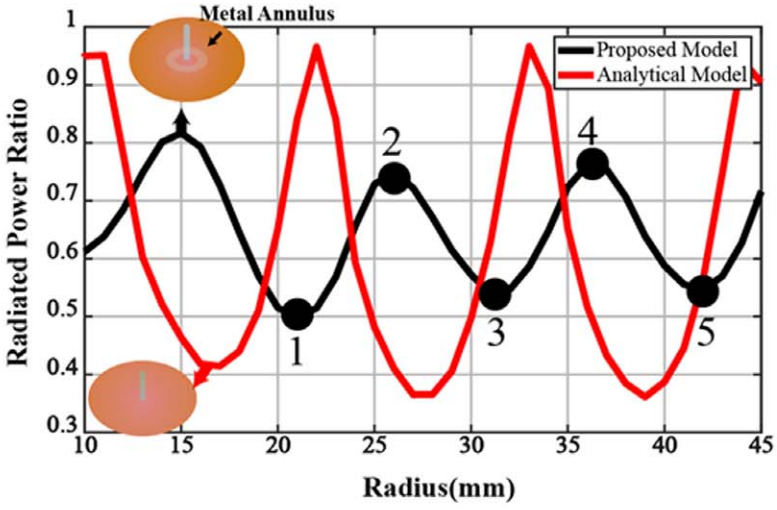

(b)

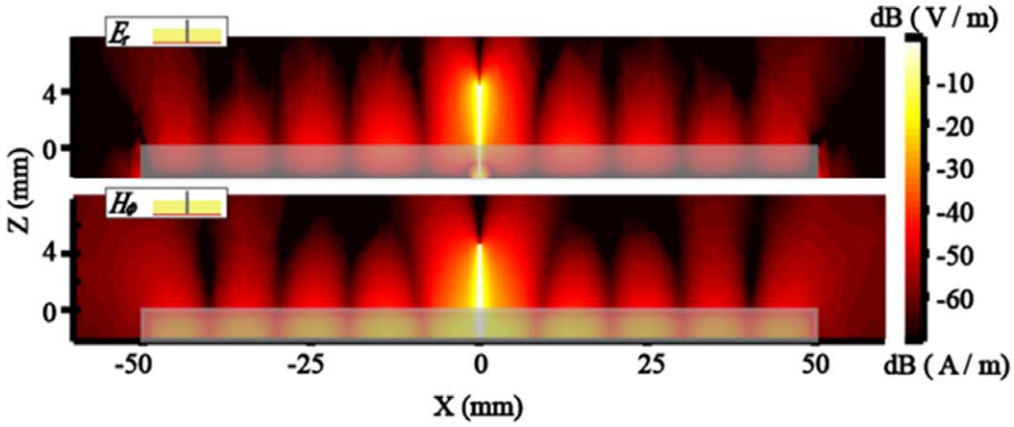

(c)

Fig. 2. (Color online) The analytical model. (a) The schematic figure of the structure. (b) Radiated power ratio with the variation of radii. The proposed model is different to the previous analytical model with an impedance matching metal annular around the probe. (c) The $\boldsymbol{E}_r$ and $\boldsymbol{H}_\varphi$ field distribution at the xoz plane at 8.5 GHz.

up to support TM_0 mode transmission only. A feeding probe at the center of the dielectric slab generates electromagnetic energy into SWMs. Note that the fundamental mode dominates because of the least attenuation. In our design, we choose the substrate RT/Duroid 6010 with a thickness of 2.54 mm and a permittivity of 10.6 backed by the same shape of a metallic ground to work at 8.5 GHz. Thus, the lowest TE mode remains insignificant since its cut-off frequency is 9.5 GHz calculated via Eq. (1) by Pozar[22)]

$$f_c = \frac{(2n-1)c}{4h\sqrt{\varepsilon_r - 1}} \quad n = 1, 2, 3, ..., \tag{1}$$

where c is the speed of light in free space, h and ε_r are the thickness and the relative permittivity of the substrate.

The radiation power ratio varies with the substrate radii, as shown in Fig. 2(b). It should be mentioned that the radiated power ratio is the radiated power over input power. The radiated power ratio is calculated under ideally lossless condition by

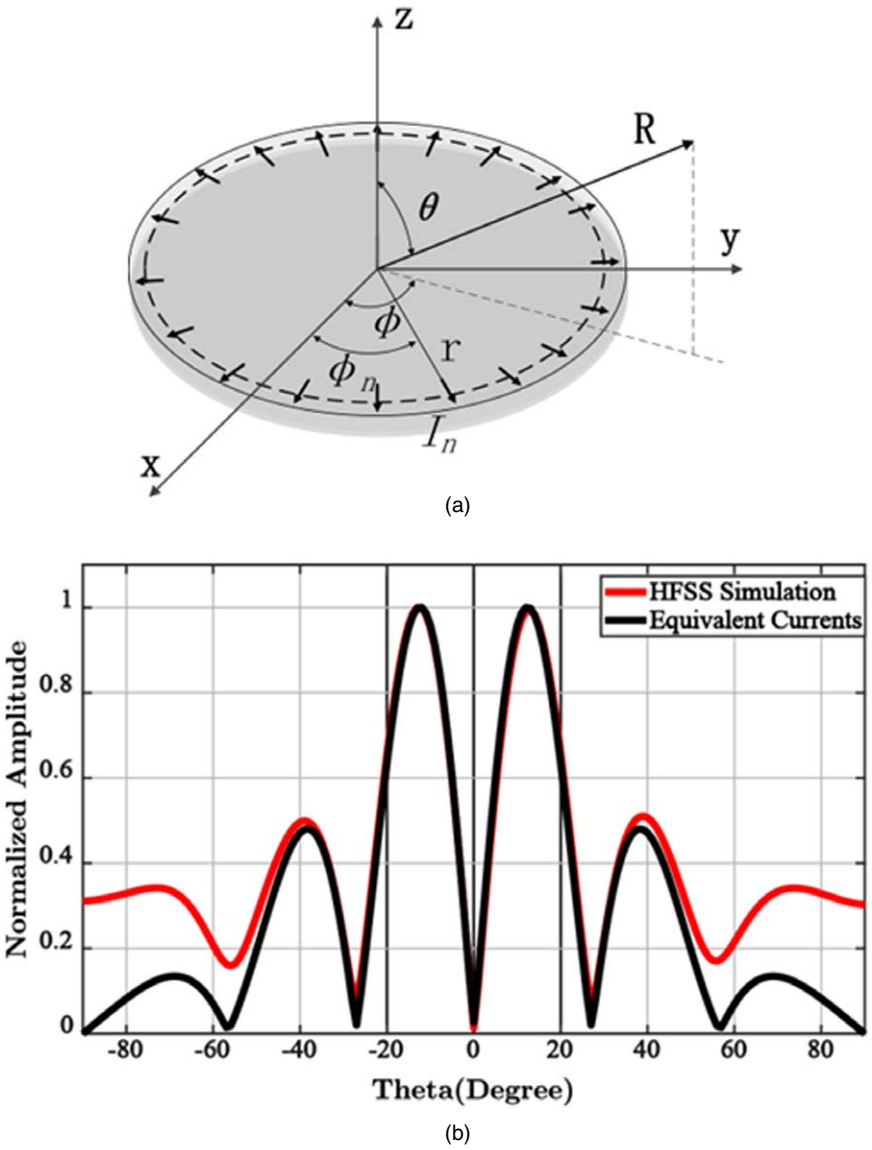

Fig. 3. (Color online) (a) The equivalent currents model. (b) Normalized radiation patterns of equivalent currents and simulation results.

Rad Power Ratio $= (P_{\text{input}} - P_{\text{reflection}})/P_{\text{input}} = 1 - |S_{11}|^2$. Different feeding structures fit different radiating properties. The analytical model (red line) has a feeding structure for a better observation of the field distributions. Meanwhile, the proposed model (black line) with the circular GDS similar to Fig. 2(a) has the same feeding structure with the Archimedean spiral and guides the Archimedean design using points 1–5 in Fig. 2(b).

This model is axially symmetric. It brings a lot of conveniences, such as TE and TM modes can be guided separately[23] in cylindrical coordinate system and the ϕ plane can be chosen arbitrarily. Since the fundamental SWM guided by the GDS is TM_0, the distributions of its components, $\boldsymbol{E_r}$ and $\boldsymbol{H_\varphi}$, are shown in Fig. 2(c), which are obtained by full-wave simulations of the commercial software *HFSS*. The interface is set at *xoy* plane. From Fig. 2(c), we can see that the source probe generates SW propagating radially along the interface. The maximum field locates at the centre of the slab. The amplitude of the SW gradually decreases along the propagation direction till the dielectric truncation.

In Fig. 2(c), the square root fallen amplitude of the surface wave presents a counter-trend of increase when approaching the truncation. Due to the diffraction and reflection of the wave, the field amplitude increases at the interface (*xoy* plane). The energy partially couples into radiation modes via diffraction. The rest of the wave is reflected between the circumference truncation and the centre-probe, resulting in a standing wave. Finally, the standing wave converts into loss and radiation. From a macro perspective, SW radiates at the discontinuities. A systematic approach of analyzing these small radiation areas is current equivalent method.

The SWDR, taken place while approaching the GDS truncation, can be regarded as a series of radially directed currents to evaluate the far field property of the surface wave. The diffraction radiation property can be estimated through the synthesis of currents array with Eqs. (2)–(5)

$$\mathbf{E}(\theta, \phi) = \sum_{n}^{N} \mathbf{I_n} G_n A_n, \tag{2}$$

$$\mathbf{I_n}(\phi) = \frac{d}{\sqrt{r}} I_0 e^{-j(l\phi_n + \phi_0)} |\cos(m\phi_n + \phi_0)| \hat{\mathbf{r}}_\mathbf{n}, \tag{3}$$

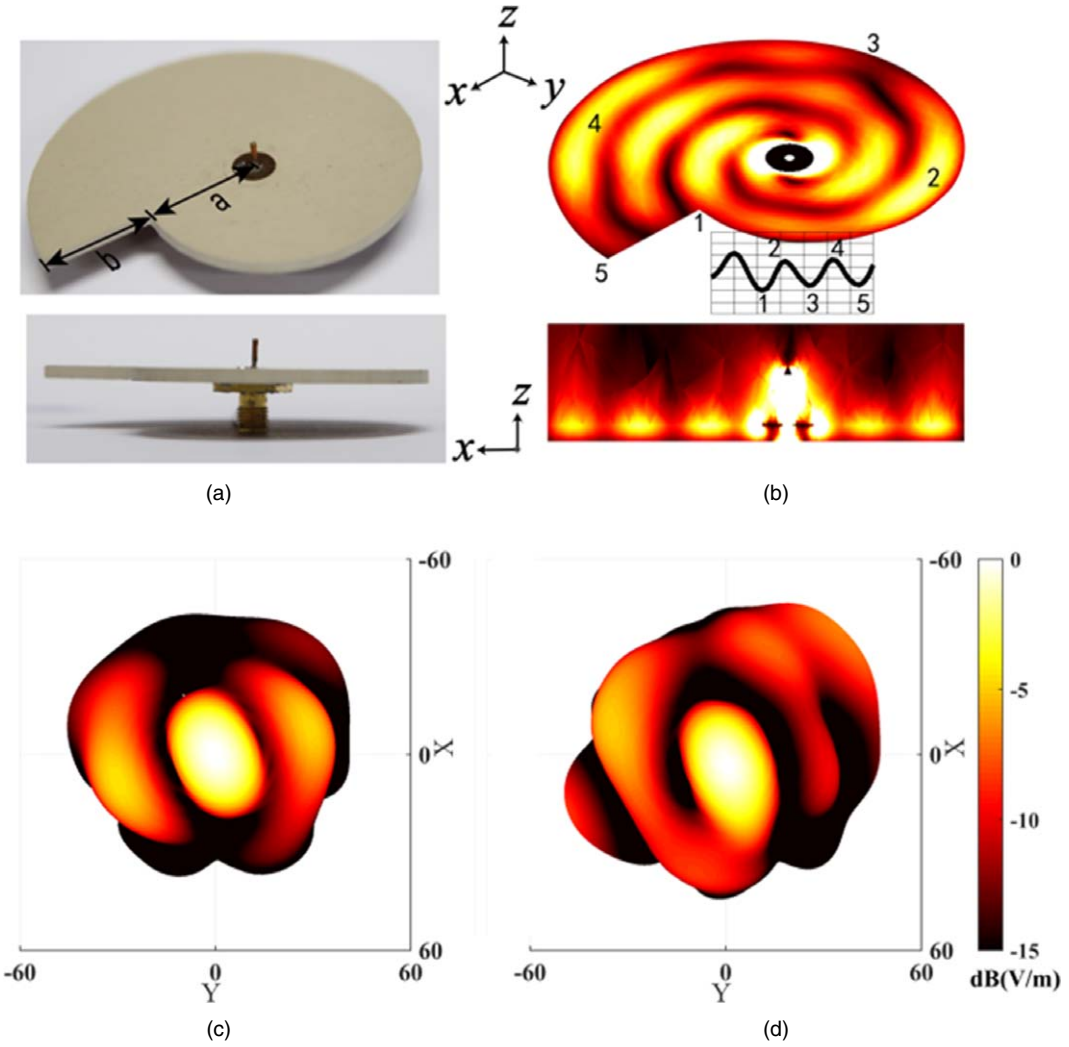

Fig. 4. (Color online) (a) Geometry of the Archimedean spiral. (b) Simulated Er field distribution. (c) Analytically calculated CP radiation pattern. (d) Measured CP radiation pattern.

$$G_n(\theta, \phi) = j\omega\mu_0 \frac{e^{-jk_0R}}{4\pi R}\sqrt{1 - \sin^2(\theta)\cos^2(\phi_n - \phi)}, \quad (4)$$

$$A_n(\theta, \phi) = e^{jk_0 r \sin(\theta)\cos(\phi_n - \phi)}. \quad (5)$$

G_n and $\boldsymbol{I}_n$ jointly determine the current element. G_n is the radiation pattern of the radially directed current, and $\boldsymbol{I}_n$ is the phase and amplitude of every element. d in Eq. (3) is the current length. A_n represents the array factor. G_n, $\boldsymbol{I}_n$ and A_n compose the power distribution in the whole space. ϕ_n is the azimuth angle of the corresponding current element. Similar to the form of orbital angular momentum, l and m in Eq. (3) represents the constants of phase and amplitude variations.

The uniform radially directed currents ($l = m = 0$) model for Fig. 2(a) are analyzed under the coordinate system shown in Fig. 3(a). Since the whole structure is symmetric with ϕ, the power distribution in the whole area can be presented by a chosen plane ($\phi = 0$). The equivalent currents radiation pattern agrees well in the vicinity of right top direction in Fig. 3(b). Because the radially directed currents have no vertical component, the major deviation caused by vertical currents appears at the azimuth plane. The Fig. 3(b) calculated by Eqs. (2)–(5) illustrates that the surface wave diffraction can be regarded as the equivalent currents to estimate the radiation property efficiently. Hence, surface wave diffraction can be served as a radiation source, shaping the expected spatial distributions of the emitted radiations.

The polarizations of $\boldsymbol{E}$ filed generated by diverse radial currents are different. Specifically, the both-side radii along one diameter share the same polarization with reverse-phase. This out-phase introduced by the radial direction shall be compensated by a 180° phase to achieve broadside radiation. Meanwhile, the CP radiation needs a series feeding phase corresponding to its azimuth angle. Since our objective is broadside CP radiation and the phase is inextricably bound to the amplitude variation, these two conditions, reflected in Eq. (3), are $l = m = 1$. Archimedean spiral shape is chosen to satisfy the value of l and m

$$r(\phi) = a + \frac{b}{2\pi}\phi. \quad (6)$$

From Fig. 2(b), we can see that the radius plays a key role in the amplitude manipulation of surface wave. To minimize the disturbance of spiral distance, $a = 22$ mm (point 1) and $2\pi b = 21$ mm (point 5 − point 1) are chosen such that the maximum field will appear at 90° (point 2) and 270° (point 4).

The proposed structure is no longer axially symmetric and the disturbance of the spiral distance is inevitable. So the radially directed currents will mix with circumferentially

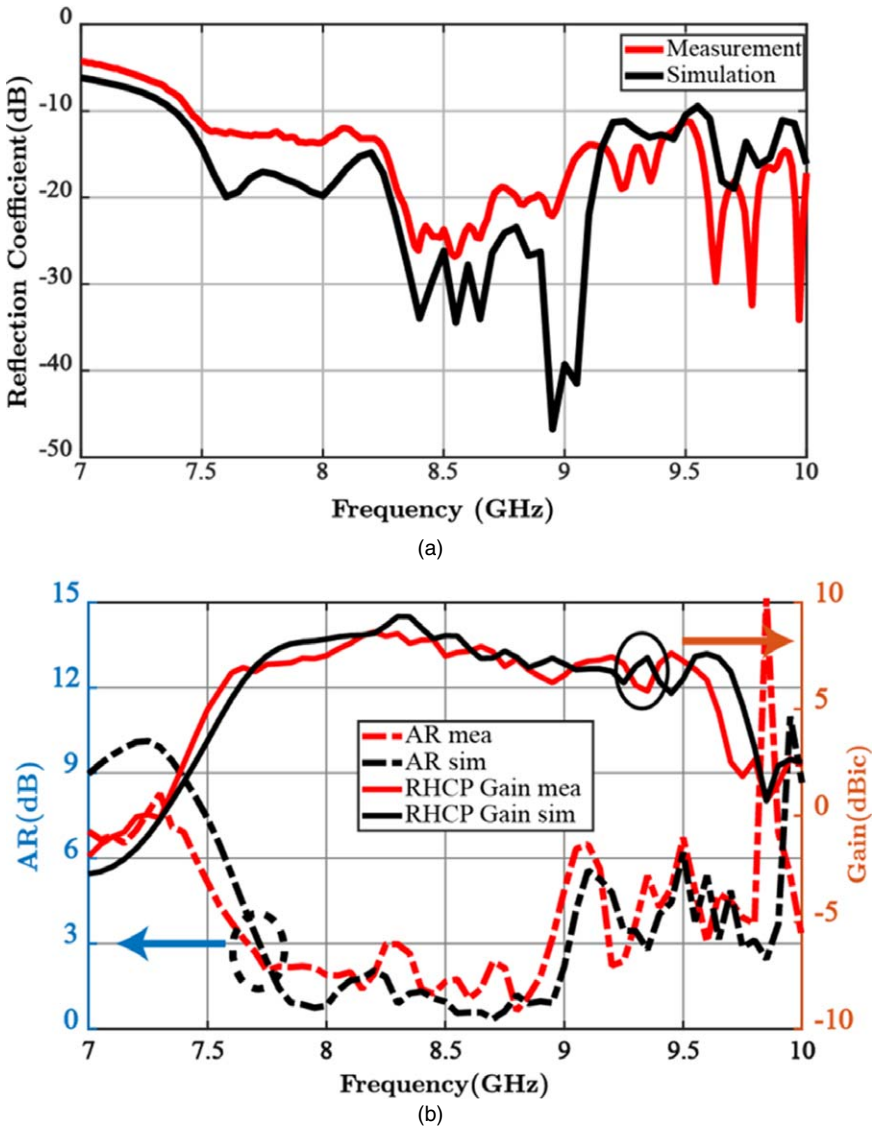

Fig. 5. (Color online) (a) The reflection coefficient of the proposed spiral GDS. (b) The broadside AR and Gain of the proposed spiral GDS.

directed components. Besides, the $\boldsymbol{E}$ and $\boldsymbol{H}$ fields are much more complicated. As a result, some approximations are adopted to simplify the analytical model, including the omission of the slight fluctuations of k_t in variation of radii. The Eqs. (2)–(5) mostly maintain the same, except the modifications of $l = m = 1$, extra circumferentially directed currents part and the radius expression adjusted in Eqs. (3) and (5)

$$\mathbf{I}_n'(\phi) = \left(\frac{1}{\sqrt{r}}\mathbf{I}_r + \frac{1}{\sqrt{a}}\mathbf{I}_\phi\right)e^{-j(\phi_n+\phi_0)}|\cos(\phi_n + \phi_0)|, \quad (7)$$

where, $\boldsymbol{I}_\phi$ is the circumferentially directed current. It is caused by the corner of the spiral distance, so square root a is used to replace r in this situation.

To verify the radiation property, a prototype is fabricated. Since a decent impedance matching is the foundation of the power coupling into SWM, in order to improve the measurement precision, the center grey metal annulus surrounding the probe is designed on the top layer of the substrate

$$A_n'(\theta, \phi) = e^{jk_0(a+b\phi_n)\sin(\theta)\cos(\phi_n-\phi)}. \quad (8)$$

Taking Eqs. (4), (7), (8) as the input of Eq. (2), we get the 3D radiation power distribution. Specifically, the comparison of the analytical and measured results with the same scale is shown in Figs. 4(c) and 4(d). There is a resonant frequency shift between measurement (8.3 GHz) and calculation (8.5 GHz). This is caused by fabrication error and material property deviation. The analytical result and the measurement results agree well in our interested right top area. Since the broadside radiation is mainly composed by the horizontal currents, we did not draw attention to the vertical currents. The diffraction mechanism leads to high side-lobe level. The other reason is that the radiating edges along the circumference formulate a large distance which is equivalent to an element spacing in the array synthesize. If the element spacing is large, a high side-lobe level will appear in the radiation pattern of the antenna. As a result of the two causes, the side lobes are high in this antenna design. They contribute the radiation in the azimuth region, and cause the main deviation from our calculation. Building a complex and detailed analytical model with the entire components will distract the focus of physical insight of the analysis, which is tending to numerical simulation.

The other relative electrical property of the proposed spiral GDS are presented in Fig. 5. The simulated and measured results meet a good agreement. The axial ratio bandwidth (ARBW) of the proposed design is from 7.7 to 8.9 GHz, or a

relative bandwidth of 14.5%. Within the entire ARBW, the right-hand CP gain is over 6.5 dBic and the reflection coefficient is below −10 dB. For the measured radiation efficiency, it is around 80% across the passband. It should be mentioned that the mainlobe is always pointing in broadside direction within the operation bandwidth.

To conclude, we verified that a broadside CP radiation can be generated using the SWDR by the centre-fed GDS with an Archimedean-spiral shape. The fundamental mode of guided SWM is TM_0, which does not radiate for the vertically decaying field upon the interface. At truncated edges, the diffraction radiation is excited. Equivalent currents method is utilized to analyze radiation property and verify the working principle of the SWDR. The good match between experimental and analytical results indicates that the proposed approach has the potential to be an alternative guide to manipulate the SWDRs.

Acknowledgments This work was supported in part by International Cooperative Research Program of Guangzhou City GDD district under Grant 2017GH21, the Research Grants Council of the Hong Kong SAR, China (Project No. CityU 11218318).

1) K. Norton, Proc. Institute Radio Eng. **25**, 1192 (1937).
2) R. E. Collin, I. Antennas, and P. Society, *Field Theory of Guided Waves* (IEEE Press, Piscataway, NJ, 1991).
3) M. Ozaki, J.-I. Kato, and S. Kawata, Science **332**, 218 (2011).
4) Z. Sun, T. Guan, W. Chen, and X. Zuo, Appl. Phys. Express **7**, 032001 (2014).
5) X. Shen and T. Jun Cui, Appl. Phys. Lett. **102**, 211909 (2013).
6) X. Shen, T. J. Cui, D. Martin-Cano, and F. J. Garcia-Vidal, Proc. Natl. Acad. Sci. **110**, 40 (2013).
7) Y. Monnai, D. Jahn, W. Withayachumnankul, M. Koch, and H. Shinoda, Appl. Phys. Lett. **106**, 021101 (2015).
8) B. Wu, H.-R. Zu, B.-Y. Xue, Y.-T. Zhao, and Q. S. Cheng, Appl. Phys. Express **12**, 022008 (2019).
9) S. Liao, C. Qi, and Q. Xue, Appl. Phys. Express **12**, 054501 (2019).
10) Z. Xu, S. Liu, S. Li, H. Zhao, L. Liu, and X. Yin, Appl. Phys. Express **11**, 042002 (2018).
11) Y.-T. Zhao, B. Wu, B.-Y. Xue, Y. Zhang, and Q. Cheng, Appl. Phys. Express **12**, 054005 (2019).
12) K. Y. Bliokh, D. Leykam, M. Lein, and F. Nori, Nat. Commun. **10**, 580 (2019).
13) G. Minatti, S. Maci, P. De Vita, A. Freni, and M. Sabbadini, IEEE Trans. Antennas Propag. **60**, 4998 (2012).
14) J. J. Xu, X. Jiang, H. C. Zhang, J. Wang, S. Qu, and T. J. Cui, Appl. Phys. Lett. **110**, 021118 (2017).
15) A. Babadjanyan, N. Margaryan, and K. V. Nerkararyan, J. Appl. Phys. **87**, 3785 (2000).
16) A. Sutinjo, M. Okoniewski, and R. H. Johnston, IEEE Trans. Antennas Propag. **58**, 675 (2010).
17) B. H. Fong, J. S. Colburn, J. J. Ottusch, J. L. Visher, and D. F. Sievenpiper, IEEE Trans. Antennas Propag. **58**, 3212 (2010).
18) K. Iizuka, M. Mizusawa, S. Urasaki, and H. Ushigome, IEEE Trans. Antennas Propag. **23**, 807 (1975).
19) C. Rusch, J. Schäfer, H. Gulan, P. Pahl, and T. Zwick, IEEE Trans. Antennas Propag. **63**, 1603 (2015).
20) H.-R. Zu, B. Wu, Y.-T. Zhao, Q. S. Cheng, and W.-B. Lu, Appl. Phys. Express **12**, 084001 (2019).
21) D. Sievenpiper, L. Zhang, R. F. Broas, N. G. Alexopolous, and E. Yablonovitch, IEEE Trans. Microwave Theory Tech. **47**, 2059 (1999).
22) D. M. Pozar, *Microwave Engineering* (Wiley, New York, 2009).
23) W. C. Chew, *Waves and Fields in Inhomogeneous Media* (IEEE Press, Piscataway, NJ, 1995).